Chemical Engineering Journal 154 (2009) 137–141

Contents lists available at ScienceDirect

Chemical Engineering Journal

journal homepage: www.elsevier.com/locate/cej

Pd substitution effects on perovskite catalyst activity for methane emission control

N. Russo*, P. Palmisano, D. Fino

Politecnico di Torino, Department of Materials Science and Chemical Engineering, Corso Duca degli Abruzzi 24, 10129 Torino, Italy

ARTICLE INFO

Article history:
Received 16 December 2008
Received in revised form 31 March 2009
Accepted 11 May 2009

Keywords:
Perovskite
Methane combustion
CNG
Pd

ABSTRACT

Perovskite-type oxides of the $LaBO_3$ and $LaB_{0.9}Pd_{0.1}O_3$ series (where B = Cr, Mn, Fe) have been prepared and characterized by X-ray diffraction (XRD), BET specific surface area, and field emission scanning electron microscope (FESEM) techniques. The activity of the reference perovskites, $LaBO_3$, and the new versions (with Pd introduction at the B-site) towards the combustion of methane, was evaluated in a Temperature Programmed Combustion (TPC) apparatus. Perovskite-type oxide containing Mn and Pd at the B-site was found to provide the best results. The half-conversion temperature of methane over the $LaMn_{0.9}Pd_{0.1}O_3$ catalyst was 425 °C, compared to 485 °C for $LaMnO_3$, with a W/F = 0.12 g s/cm^3. On the basis of a Temperature Programmed Desorption (TPD) analysis of oxygen as well as catalytic combustion runs, the prevalent activity of the $LaMn_{0.9}Pd_{0.1}O_3$ catalyst could be explained by its capability to deliver a higher amount of intrafacial oxygen. This catalyst was then deposited on cordierite monoliths in a γ-Al_2O_3 supported form (catalyst weight percentage 15%) and tested in a lab-scale test rig under realistic conditions. Half methane conversion (T_{50}) was achieved at 340 °C (Gas Hourly Space Velocity (GHSV) = 10 000 h^{-1}), almost the same T_{50} value as the commercial 4 wt% Pd/γ-Al_2O_3 catalyst, but with a six-times lower amount of the expensive noble metal.

1. Introduction

From the environmental point of view, Compressed Natural Gas (CNG) engines could lead to very low pollutant emissions. However, unburned methane is harder to oxidise than gasoline-derived unconverted HCs. The strong greenhouse effect of methane (more than one order of magnitude higher than that of CO_2) has induced increasing concern at a legislation level and led to the development of tailored after-treatment technologies [1–3]. Catalytic combustion of methane on honeycomb converters similar to those used for the treatment of gasoline engine exhaust gases is the route that should be taken to resolve this problem. Particular demands are imposed on the catalysts used for methane combustion. They must resist thermal and mechanical shocks and exhibit high activity, which is not trivial due to the high stability of CH_4 and the low temperature of CNG vehicle exhausts (which rarely exceed 500 °C). Commercial catalysts are based above all on γ-Al_2O_3-supported Pd [4–7], which have at least a three-times higher noble metal loading compared to those of conventional three-way catalysts. However, besides being expensive, the latter sinter easily. A possible solution could be the insertion of the noble metal into a perovskite-type transition metal oxide structure which, in our tests, when properly prepared, resulted to be comparably active, highly resistant to deactivation and much cheaper.

Perovskites are mixed oxides of the general formula: $ABO_{3\pm\delta}$, where A is usually a lanthanide ion and B is a transition metal ion. Both A and B can be partially substituted, leading to a wide variety of mixed oxides of the general formula: $A_{1-x}A'_xB_{1-y}B'_yO_{3\pm\delta}$, characterized by structural and electronic defects, due to their non-stoichiometry, which is indicated by the subscript δ in the formula. For full oxidation reactions, such as methane combustion, cation B is considered to be responsible for the catalytic activity [8], while cation A, especially when partially substituted by a cation A′ of different valence, governs the formation of crystal lattice vacancies and can stabilize unusual oxidation states for B, leading to different catalytic performances [8–10]. The oxidation activity of perovskites has been ascribed to their ionic conductivity, to oxygen mobility within their lattice [9], to their reducibility and to their oxygen sorption properties [11]. Two possible mechanisms, a suprafacial and an intrafacial one, were in fact proposed some time ago [12] and are now widely accepted for the oxidation reactions over these catalysts. The former mechanism arises from the interaction of surface oxygen with the reactants and it is operative at low temperatures (<400 °C). The latter is effective at higher temperatures (>400 °C) and involves a Mars–Van Krevelen redox cycle. In it, bulk lattice oxygen migrates towards the surface, becoming available for the oxidation of the adsorbed substrate and is quickly replaced by oxygen from the gaseous phase. The mobility of O^{2-} ions within the

* Corresponding author. Tel.: +39 011 5644710; fax: +39 011 5644699.
E-mail address: nunzio.russo@polito.it (N. Russo).

1385-8947/$ – see front matter © 2009 Elsevier B.V. All rights reserved.
doi:10.1016/j.cej.2009.05.015

crystalline framework determines the catalytic reaction mechanism [10].

A research programme carried out at Politecnico di Torino was aimed at developing nanostructured Pd-perovskite-type-oxide catalysts employing a markedly smaller or similar overall noble metal load than that used in conventional converters. The present manuscript deals with the development of these catalysts. The performance of the most promising developed catalyst, once deposited on a honeycomb catalytic converter and tested in a lab-scale test rig, is also presented and discussed.

2. Experimental

2.1. Catalyst preparation and characterization

A series of perovskite catalysts ($LaMnO_3$, $LaMn_{0.9}Pd_{0.1}O_3$, $LaFeO_3$, $LaFe_{0.9}Pd_{0.1}O_3$, $LaCrO_3$, and $LaCr_{0.9}Pd_{0.1}O_3$) were prepared via a highly exothermic and self-sustaining reaction, the so-called "Solution Combustion Synthesis" (SCS) method [13]. This technique is particularly suitable for producing nanosized particles and entails the formation of pure oxide catalysts with rather high specific surface areas in the absence of any carrier. This allows the intrinsic catalytic activity of the prepared compound series to be compared more easily.

A crucible containing a concentrated aqueous solution of various precursors (metal nitrates and urea) was placed in an oven at 600 °C for a few minutes, in order to ignite the very fast synthesis reactions. All the catalysts were then ground in a ball mill and characterized by different analyses (XRD - PW1710 Philips diffractometer equipped with a monochromator for the Cu-K_α radiation, FESEM - Leo 50/50 VP with Gemini column) in order to check that the desired microstructure and chemical composition were obtained. The activity of the prepared catalysts was analyzed through Temperature Programmed Combustion (TPC), according to the following standard screening operating procedures: a gas mixture (2.5 vol.% CH_4; 7.5 vol.% O_2, He = balance) was fed at the constant rate of 0.83 N ml s^{-1} to a fixed-bed reactor constituted of 100 mg of powdered catalyst and 900 mg of silica pellets (0.3–0.7 mm in size) (W/F = 0.12 g s/cm^3). This inert material (SiO_2) was adopted to reduce the specific pressure drop across the reactor and to prevent thermal runaways. Starting from 950 °C, the inlet temperature, measured by a K-type thermocouple placed alongside the quartz tube, was decreased at a 2 °C/min rate and the outlet CO_2, CO, CH_4 and O_2 concentrations were determined using continuous Non-Dispersive Infrared Sensor (NDIR) and paramagnetic analyzers, thus allowing the methane conversion to be calculated and the carbon balances to be closed (relative error: ±4%). Methane half-conversion temperatures (T_{50}) were evaluated from the obtained typical sigma-shaped curves, as an index of the catalytic activity towards methane combustion. Each data point was obtained as the average of three twin runs performed on different samples of the same catalytic material. In order to fully appreciate the catalytic effect of the perovskites, blank runs were also carried out in the absence of the catalyst and in the presence of just SiO_2.

Some further analyses were performed on the prepared perovskite catalysts in a Temperature Programmed Desorption/Reduction/Oxidation (TPD/R/O) analyzer, equipped with a thermal conductivity (TCD) detector (TPD/R/O 1100 Thermoquest). A fixed catalyst bed was enclosed in a quartz tube and sandwiched between two quartz wool layers; the catalyst was heated under an O_2 flow (40 N ml/min) up to 750 °C before each Temperature-Programmed Desorption (TPD) run. After 30 min at this temperature, as a common pretreatment, the fixed bed temperature was then lowered to room temperature with the same oxygen flow rate, thereby allowing complete oxygen adsorption over the catalyst. Helium was then fed to the reactor at a rate of 10 ml/min, which was maintained for 1 h at room temperature to purge any excess oxygen molecules. The catalyst was then heated to 900 °C at a constant rate of 10 °C/min under a helium flow rate of 10 N ml/min. A detailed description of the Temperature Programmed Desorption of the oxygen analysis is reported in Ref. [8]. X-ray diffraction was once again performed on the catalysts which underwent TPD analysis, to check whether the perovskite structure had been retained or not, and to check for the possible appearance of new phases.

2.2. Catalytic monolith preparation and characterization

The catalytic converters (cylindrical cordierite honeycombs by Chauger; cell density: 200 cpsi; length: 25 mm; diameter: 34 mm) were prepared by a preliminary deposition of a layer of γ-alumina by *in situ* SCS [14] (10 wt% referring to the monolith weight) followed by deposition of 15 wt% (referring to the γ-alumina weight) of $LaMn_{0.9}Pd_{0.1}O_3$, the most active perovskite catalyst. Adhesion tests and a structural characterization (XRD, FESEM) were carried out. The adhesion properties between the catalyst and the ceramic surface were checked by means of an ultrasonic bath test: a piece of the catalytic monolith was weighed before and after a standard ultrasonic treatment [15] to quantify the catalyst loss. A physical–chemical characterization was performed on sections of the catalyzed monolith; in particular, field emission scanning electron microscopy (FESEM) analyses were performed using a FESEM - Leo 50/50 VP with GEMINI column apparatus equipped with an energy-dispersive spectrometer, in order to investigate the morphology and composition of the deposited catalytic layer. Catalytic combustion experiments were performed in a stainless steel reactor heated in a horizontal split tube furnace [15] characterized by a 60 cm heating length. The catalyzed monolith was sandwiched between two mullite foams to optimize flow distribution. A thermocouple, inserted along one of the central monolith channels, was used for the temperature control to measure the inlet temperature.

Lean inlet conditions (0.4 vol.% CH_4, 10 vol.% O_2, N_2 balance) were ensured via mass flow controllers. The GHSV was set equal to 10 000, 40 000 and 80 000 h^{-1}, whereas the composition of the off-gases was monitored using the same analyzing equipment described above.

A converter containing 4 wt% of Pd-γ-alumina, simulating a commercial catalyst was also prepared by impregnation of a bare γ-alumina coated monolith and tested under the previous reference conditions.

3. Results and discussion

The XRD spectra (Fig. 1) of the prepared perovskite catalysts showed diffraction peaks corresponding to the desired structure of the catalysts (JPCDS card: PDF 24-1016 for $LaCrO_3$, JPCDS card:

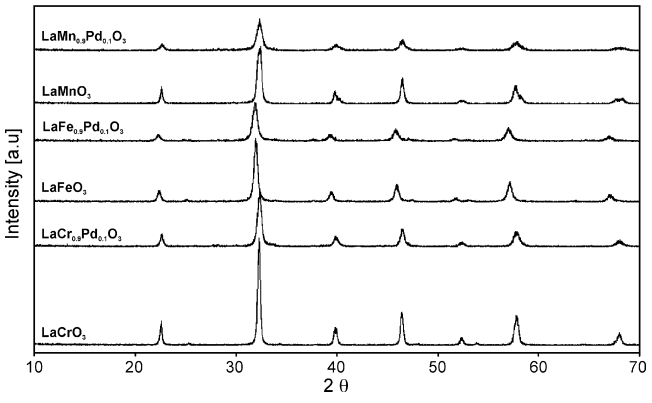

Fig. 1. XRD diffraction patterns of the perovskite-type catalysts.

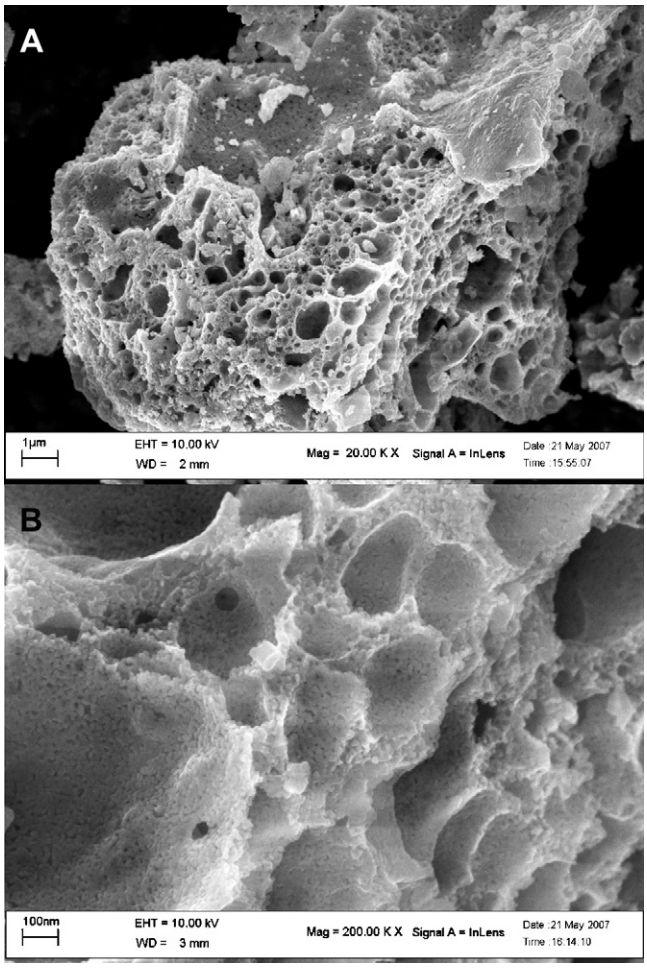

Fig. 2. Electron microscopy results concerning the $LaMn_{0.9}Pd_{0.1}O_3$ catalyst in powder: (A) FESEM view of the catalyst microstructure and (B) FESEM view of the catalyst crystals.

PDF 74-2203 for $LaFeO_3$ and JPCDS card: PDF 89-0644 for $LaMnO_3$); no diffraction peaks were detected related to the other phases. This confirms, for the substituted perovskite samples, that the insertion of Pd as a cation inside the crystalline structure was obtained.

Fig. 2A shows an FESEM micrograph of the $LaMn_{0.9}Pd_{0.1}O_3$ perovskite-type catalyst which refers to the catalyst that showed the highest activity among those prepared. The foamy morphology of the catalyst is a consequence of the rapid generation of gases during the combustion synthesis, due to the decomposition/combustion of the reacting precursors. Such a structure should enable a good internal mass rate to be obtained. Fig. 2B shows an FESEM micrograph regarding the same catalyst observed with a higher magnification. Most of the perovskite crystals range between 40 and 100 nm in size, which is in accordance with the BET specific surface areas measured (10–30 m^2/g), reported in Table 1. It can in fact easily be calculated that the above range size should correspond approximately to specific surface areas in the 8–23 m^2/g range, once the average density of the catalyst particles equal to 6500 kg/m^3 [16], an average value for the tested perovskites, and a spherical shape for the particles themselves are assumed. Finally, no indications on the possible presence of amorphous or minor crystalline phases are perceivable in Fig. 2B, in any FESEM observation made on $LaMn_{0.9}Pd_{0.1}O_3$ or any other catalyst.

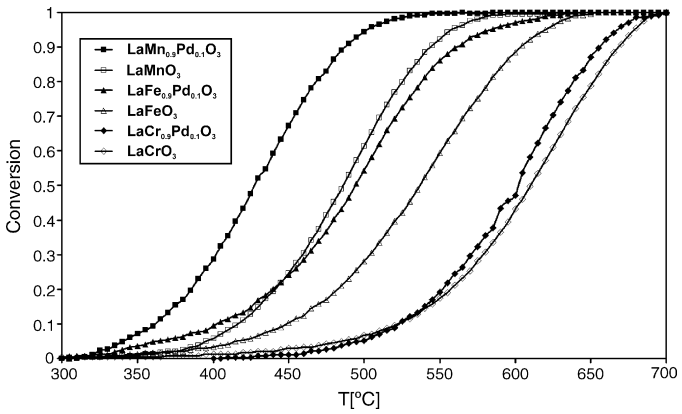

Fig. 3. Methane conversion vs. temperature plots: comparison of the perovskite catalysts.

Fig. 3 illustrates the methane conversion vs. temperature plots recorded for the catalysts considered. All the catalysts assured much lower T_{50} values than the one related to non-catalytic combustion (816 °C—not reported). The $LaMn_{0.9}Pd_{0.1}O_3$ catalyst offered the best performance with a T_{50} value of 425 °C. However, it is worthwhile noting that an improvement of the activity was observed for all the catalysts by inducing a partial substitution with 10% of Pd at the B-site. In other words, the T_{50} of the Pd substituted perovskites was lowered by 5, 40 and 60 °C, respectively, from $LaCrO_3$ to $LaCr_{0.9}Pd_{0.1}O_3$, from $LaFeO_3$ to $LaFe_{0.9}Pd_{0.1}O_3$ and from $LaMnO_3$ to $LaMn_{0.9}Pd_{0.1}O_3$.

This result cannot be explained on the basis of the BET specific surface area values since the perovskites obtained by Pd partial substitution of the Mn, Cr and Fe from the mother $LaBO_3$ exhibited lower specific surface area values than those of the non-substituted Pd counterparts. Transient thermal analysis studies (TPD) were quite helpful to better elucidate this issue. As thoroughly discussed in a review by Seyama [17], perovskites can desorb two different types of oxygen species at high temperatures: a low temperature species, named α, desorbed in the 300–600 °C range, and a high-temperature one, named β, desorbed above 600 °C. The α desorption peak is not always perceivable in TPD plots and depends to a great extent on the concentration of the surface oxygen vacancies. Its onset and intensity depend primarily on the degree of substitution of the A ion with ions of lower valence but also on the nature of the B metal of the ABO_3 structure [8]. Conversely, the β peak is closely related to the nature of the B ion and its occurrence is closely linked to redox transitions of the valence state of this ion. If the oxygen TPD plots of the prepared catalysts are compared (Fig. 4), a significant difference can be noticed.

Table 1
Half-conversion temperatures of methane, BET specific surface area values and specific molecular mass of the desorbed α- and β-oxygen species referring to the fresh catalysts.

	T_{50} (°C)	BET surface area (m^2/g)	Desorbed α-oxygen (μmol/g)	Desorbed β-oxygen (μmol/g)
No catalyst	816	–	–	–
$LaFeO_3$	535	17.4	1.1	4.1
$LaFe_{0.9}Pd_{0.1}O_3$	495	11.6	11.0	81.0
$LaMnO_3$	485	8.1	17.2	176.3
$LaMn_{0.9}Pd_{0.1}O_3$	425	7.2	17.0	240.1
$LaCrO_3$	615	26.1	21.2	18.6
$LaCr_{0.9}Pd_{0.1}O_3$	610	22.3	29.2	18.9

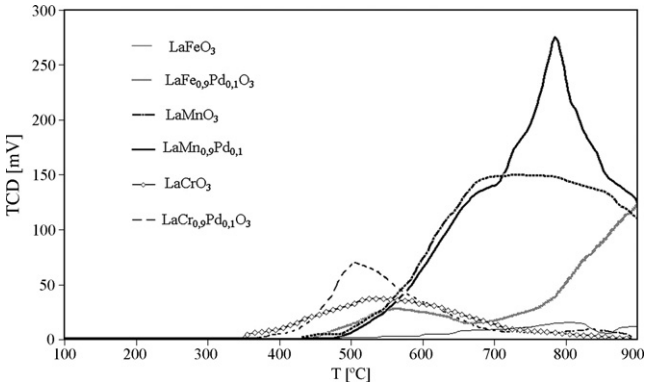

Fig. 4. Results of the oxygen Temperature Programmed Desorption (TPD) tests on the pure perovskite catalysts.

The oxygen desorption peak that occurs above 600 °C for $LaMnO_3$ is larger in the Mn-substituted perovskite ($LaMn_{0.9}Pd_{0.1}O_3$). These types of oxygen species, generally known as β-oxygen (intrafacial oxygen—desorbed above 600 °C) in the reference literature [14,15], are probably more reactive than the α-oxygen desorbed in the lower temperature range (suprafacial oxygen—desorbed below 600 °C). According to most studies in the field [17], the β-oxygen belonging to the perovskite lattice can be exploited for the catalytic conversion of methane. The results obtained from the TPD analysis clearly illustrate a correlation between the catalytic activity order and the capability to desorb a larger amount of β-oxygen. The specific molecular mass of the desorbed α- and β-oxygen species determined from the curves in Fig. 4 is listed in Table 1: the larger the β-oxygen desorbed the lower T_{50}. Moreover, it is clear that the deposition of Pd on a surface involves the formation of Pd/PdO clusters (4 wt% Pd on γ-Al_2O_3). Conversely, the introduction of Pd inside the perovskite crystalline structure entails the presence of Pd cations, thus increasing the number of specific active sites.

Fig. 5 shows an FESEM micrograph of a γ-Al_2O_3 carrier/$LaMn_{0.9}Pd_{0.1}O_3$ perovskite-type catalyst deposited onto the cordierite monolith channels via *in situ* SCS. Its microstructure is foamy. During the SCS process, the decomposition–combustion of both γ-Al_2O_3 and $LaMn_{0.9}Pd_{0.1}O_3$ reacting precursors generates a large amount of gaseous products in a very short period of time, which leads to a final spongy morphology. This feature favours the formation of large intra-layer pores for the catalyst cluster agglomerates, which reduces the mass transfer resistance of the layer itself.

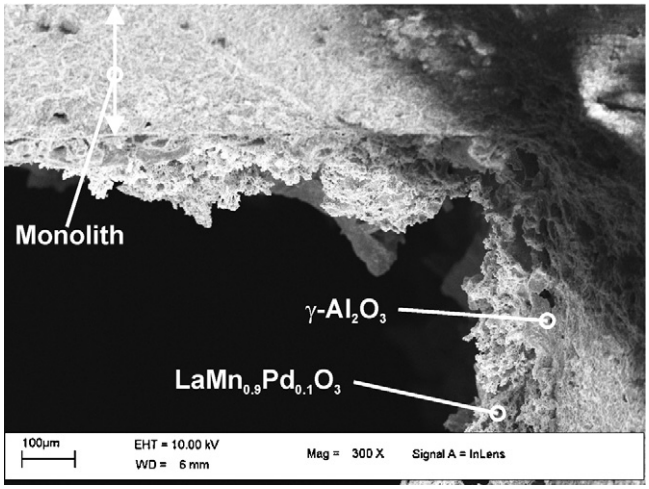

Fig. 5. FESEM views of the γ-Al_2O_3–$LaMn_{0.9}Pd_{0.1}O_3$ catalyst layer deposited over a cordierite honeycomb.

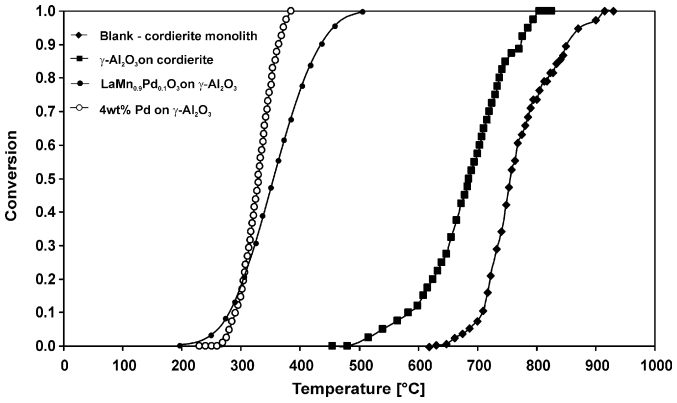

Fig. 6. Methane conversion, as a function of temperature, over different catalysts deposited on the cordierite monolith (GHSV = 10 000 h^{-1}).

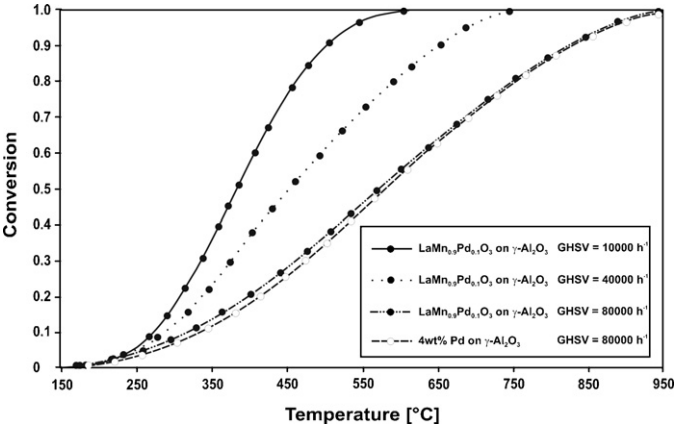

Fig. 7. GHSV effect on the catalytic performance of the γ-Al_2O_3–$LaMn_{0.9}Pd_{0.1}O_3$ perovskite-type catalyst. 4 wt% Pd on γ-Al_2O_3 (GHSV = 80 000 h^{-1}) for comparison purposes.

The adhesion between the deposited catalyst and the trap channel walls was excellent, as the loss of catalyst through the ultrasonic treatment was lower than 1%.

The methane conversion curves (GHSV = 10 000 h^{-1}) plotted in Fig. 6 vs. temperature over different catalysts deposited on a cordierite monolith show that the monolith with the internal γ-Al_2O_3 layer induced a slight improvement of the activity compared to the blank one. The presence of the $LaMn_{0.9}Pd_{0.1}O_3$ catalyst enabled a determinedly better T_{50} decrease by shifting this temperature to 340 °C, a performance similar to that of the conventional 4 wt% Pd/γ-Al_2O_3 catalyst, but guaranteed with just a six-times lower noble metal load.

The methane conversion curves plotted in Fig. 7 vs. temperature at three different GHSVs showed that the conversion curve shifted to lower temperatures at lower space velocities, with T_{50} values of 570, 455 and 385 °C at GHSV of 80 000, 40 000 and 10 000 h^{-1}, respectively. The catalytic performance of the monolith supporting the conventional 4 wt% Pd/γ-Al_2O_3 catalyst at the highest GHSV (80 000 h^{-1}), which is representative of real conditions [18], is quite similar to the catalytic performance of γ-Al_2O_3–$LaMn_{0.9}Pd_{0.1}O_3$, confirming that the insertion of the noble metal inside the perovskite crystalline structure is the right way to reduce the amount of noble metal and the relative costs.

4. Conclusions

Several perovskite-type-oxide catalysts ($LaMnO_3$, $LaMn_{0.9}Pd_{0.1}O_3$, $LaFeO_3$, $LaFe_{0.9}Pd_{0.1}O_3$, $LaCrO_3$, and $LaCr_{0.9}Pd_{0.1}O_3$) have

been prepared by solution combustion synthesis, characterized, and tested as catalysts for methane combustion. Specific experiments were carried out with pure perovskites in powder to compare their activity towards methane combustion. The screening tests demonstrated a superior activity towards methane conversion by inducing a partial substitution of the perovskite B-site with Pd: the best catalyst was found to be $LaMn_{0.9}Pd_{0.1}O_3$ (T_{50} = 425 °C) and it was therefore selected to be deposited and tested on a cordierite monolith.

Experimental tests on an *ad hoc* prepared CNG exhaust gas aftertreatment converter have confirmed the good performance of the selected $LaMn_{0.9}Pd_{0.1}O_3$ catalyst, even in the structured form. This should entail a noticeable reduction of the overall costs of catalysts compared to the conventional Pd-only catalysts that are currently employed with six times higher Pd loads. Specific activities are currently in progress both to develop more active perovskite catalysts and to optimize the amount of Pd in order to gain a further reduction in this costly noble metal in catalyst formulation.

References

[1] Web site: www.epa.gov.
[2] Transportation Research Board, Toward a sustainable future. Addressing the long-term effects of motor vehicle transportation on climate and ecology, Special Report 251, National Academy Press, Washington, 1997.
[3] Web site: www.eia.doe.gov, Electric power industry generation by energy source, Electric Power Annual 1998, vol. II, Table 1, pp. 3–12.
[4] I. Cerri, M. Pavese, G. Saracco, V. Specchia, Premixed metal fibre burners based on a Pd catalyst, Catalysis Today 83 (2003) 19–31.
[5] P. Forzatti, G. Groppi, Catalytic combustion for the production of energy, Catalysis Today 54 (1999) 165–180.
[6] D.L. Mowery, M.S. Graboski, T.R. Ohno, R.L. McCormick, Deactivation of $PdO–Al_2O_3$ oxidation catalyst in lean-burn natural gas engine exhaust: aged catalyst characterization and studies of poisoning by H_2O and SO_2, Applied Catalysis B: Environmental 21 (1999) 157–169.
[7] J.K. Lampert, M.S. Kazi, R.J. Ferrauto, Palladium catalyst performance for methane emissions abatement from lean burn natural gas vehicles, Applied Catalysis B: Environmental 14 (1997) 211–223.
[8] N. Yamazoe, Y. Teraoka, Oxidation catalysis of perovskites, relationships to bulk structure and composition, Catalysis Today 8 (1990) 175–199.
[9] M.S. Islam, M. Cherry, C.R.A. Catlow, Oxygen diffusion in $LaMnO_3$ and $LaCoO_3$ perovskite-type oxides: a Molecular Dynamics Study, Journal of Solid State Chemistry 124 (1996) 230–237.
[10] R. Leanza, I. Rossetti, L. Fabbrini, C. Oliva, L. Forni, Perovskite catalysts for the catalytic flameless combustion of methane: preparation by flame-hydrolysis and characterization by TPD–TPR-MS and EPR, Applied Catalysis B: Environmental 28 (2000) 55–65.
[11] L.G. Tejuca, J.L.G. Fierro, Properties and Applications of Perovskite-type Oxides, Marcel Dekker Eds., New York, 1993.
[12] I. Rossetti, L. Forni, Catalytic flameless combustion of methane over perovskites prepared by flame-hydrolysis, Applied Catalysis B: Environmental 33 (2001) 345–352.
[13] A. Civera, M. Pavese, G. Saracco, V. Specchia, Combustion synthesis of perovskite-type catalysts for natural gas combustion, Catalysis Today 83 (2003) 199–211.
[14] D. Fino, N. Russo, G. Saracco, V. Specchia, CNG engines exhaust gas treatment via Pd-spinel-type-oxide catalysts, Catalysis Today 117 (2006) 559–563.
[15] D. Fino, N. Russo, G. Saracco, V. Specchia, Supported Pd-perovskite catalyst for CNG engines exhaust gas treatment, Progress in Solid State Chemistry 35 (2007) 501–511.
[16] R.H. Perry, D.W. Green, J.O. Maloney, Perry's Chemical Engineers' Handbook, VI ed., McGraw-Hill Book Co., New York, 1984.
[17] T. Seyama, Total oxidation of hydrocarbon on perovskite oxide, Catalysis Reviews: Science and Engineering 34 (1992) 281–300.
[18] G.C. Koltsakis, A.M. Stamatelos, Catalytic automotive exhaust after treatment, Progress Energy Combustion Science 23 (1997) 1–39.